

Using Combined PIC and MHD to Model Particle Acceleration in Galaxy Cluster Shocks^{*})

Allard Jan VAN MARLE, Dongsu RYU, Hyesung KANG¹⁾ and Ji-Hoon HA

Department of Physics, UNIST, UNIST-gil 50, Ulsan 44919, Korea

¹⁾*Department of Earth Sciences, Pusan National University, Busan 46241, Korea*

(Received 20 December 2018 / Accepted 10 May 2019)

When clusters of galaxies merge, shocks are formed that are characterized by a low (1-4) sonic Mach number and an Alfvénic Mach number that is typically an order of magnitude higher, giving the shocks a plasma β of approximately 100. The question we seek to answer is to what extent shocks can accelerate particles to relativistic speeds and thereby contribute to the cosmic ray spectrum. We use a combined particle-in-cell and magnetohydrodynamics code, which treats the thermal plasma as a fluid, but uses a kinetic approach to deal with non-thermal particles. This approach is computationally cheaper than the traditional PIC method while preserving the ability to deal with non-thermal particles. Our preliminary results confirm the ability of shocks in the low-Mach, high- β regime that characterizes galaxy cluster merger shocks to accelerate particles depends strongly on the input parameters, which was previously shown with PIC simulations.

© 2019 The Japan Society of Plasma Science and Nuclear Fusion Research

Keywords: astrophysical shock, galaxy cluster, particle acceleration, method, numerical

DOI: 10.1585/pfr.14.4406119

1. Introduction

When two clusters of galaxies collide, the interaction creates a shock. These shocks are typically weak, with sonic Mach numbers (M_s) of 1-4 because of the hot, intra-cluster medium (ICM) e.g. [1, 2]. However, because the intra-cluster magnetic field is usually weak, they tend to have an Alfvénic Mach number (M_A) about one order of magnitude higher, leading to a typical plasma- β (the ratio of thermal to magnetic pressure) of approximately 100.

These galaxy cluster merger shocks are thought to accelerate cosmic ray (CR) protons and electrons through diffusive shock acceleration (DSA), also known as Fermi I acceleration e.g. [3–5], a process which occurs when a particle repeatedly crosses the shock after being reflected by a turbulent magnetic field. However, as yet there has been no observational confirmation of CR ions that have been accelerated by shocks between galaxy clusters (E.g. see [6–8]). If these ICM shocks produce CR protons, inelastic collisions between such CR protons and thermal protons followed by neutral pion decay would result in diffuse gamma-ray emission. However, Fermi-LAT [9] has not detected this. Cosmological hydrodynamics simulations by [10] led to the conclusion that the non-detection by Fermi-Lat provides an upper limit for the CR acceleration efficiency of 10^{-3} for galaxy cluster collision shocks with $M \approx 1-5$.

In order for a shock to accelerate particles it is necessary that the magnetic field is perturbed sufficiently that

particles moving away from the shock can be reflected back toward the shock by the magnetic field. This is a condition that can be created by the supra-thermal particles themselves, which trigger turbulent waves as they move away from the shock in the upstream direction. The process of particle acceleration in astrophysical shocks has been investigated numerically using a variety of methods, such as the particle-in-cell (PIC) hybrid method (E.g. [12–14]), which treats the electrons as a fluid, and the ions as particles. The conclusion obtained from such simulations is that quasi-parallel shocks (where the magnetic field makes an angle of less than 45° with the direction of the flow) can effectively accelerate particles to relativistic speeds but that quasi-perpendicular shocks (where the angle is more than 45°) are incapable of doing so. An alternative model, using a combination of PIC and magnetohydrodynamics (MHD) [15] showed that particle acceleration by quasi-perpendicular shocks might be possible, provided that the initial injection rate of supra-thermal particles at the shock is sufficiently high.

The models described above have focused primarily on strong, low- β (~ 1) shocks of the type expected for colliding stellar winds and expanding supernova remnants, rather than the weak, high- β shocks that occur in the ICM. PIC simulations of weak, quasi-parallel shocks with high plasma- β by [16] showed that for weak shocks the *injection process*, which energizes thermal particles to supra-thermal energies, depends strongly on the sonic Mach number. Injection of supra-thermal ions involves a multi-step process. Initially, ions are reflected at the shock front and accelerated by shock-drift acceleration (SDA). These

author's e-mail: vanmarle@unist.ac.kr

^{*}) This article is based on the presentation at the 2nd Asia-Pacific Conference on Plasma Physics (AAPPS-DPP2018).

ions move upstream along the magnetic field and excite waves in the upstream medium. Once these waves perturb the magnetic field sufficiently to cause deviations in the direction of the field, they can reflect the ions back toward the shock. According to [16] for shocks with $M_s \leq 2.25$, the injection rate of supra-thermal particles drops by an order of magnitude from 3×10^{-3} at $M_s \leq 2.25$ to 3×10^{-4} at $M_s \leq 2.0$. This critical Mach number is significantly higher than the analytic prediction based on the Rankine-Hugoniot conditions [17], which placed the critical Mach number at $M_s \approx 1.1$ and may help to explain the lack of observed diffuse gamma-rays produced in high- β ICM shock accelerated ions.

We continue these simulations, using a different numerical method that combines both PIC and grid-based MHD [11, 15, 18, 19]. Henceforth this method will be referred to as Particles in MHD Cells (PI[MHD]C). This method is based on the assumption that an astrophysical plasma can be described as a primarily thermal plasma, which can be described with a fluid-approach, and a relatively small supra-thermal component, which has to be treated kinetically. That being the case, the numerical work can be split, with the thermal plasma being simulated with MHD and the supra-thermal particles being treated using PIC. For this particular model, we only use non-thermal ions. The electrons are assumed to be fully thermalized. This approach allows us to take advantage of the high computational efficiency of MHD, while maintaining the ability to simulate the motion of individual supra-thermal particles. We take advantage of this by performing 2-D simulations in order to investigate the shock structure.

2. Method

We use the well-known MPI-AMRVAC code, e.g. [20], which is a fully conservative, MPI-parallel finite-volume code that solves the conservation equations of mass, momentum, and energy on an adaptive grid. It uses the OCTREE [21] method to dynamically refine and coarsen the mesh depending on local conditions of the thermal plasma.

To this code we have added a new module that incorporates both the supra-thermal particles as well as the additions to the conservation equations of the thermal plasma [15]. The two components (thermal and supra-thermal) interact through the electromagnetic field. (There is no CR pressure term in the conservation equations.) For each particle, the equation of motion is given by

$$\frac{\partial \mathbf{p}_j}{\partial t} = q_j \left(\mathbf{E} + \frac{\mathbf{u}_j}{c} \times \mathbf{B} \right), \quad (1)$$

with \mathbf{p}_j , q_j and \mathbf{u}_j the momentum, charge, and velocity of the particle with index j and \mathbf{B} and \mathbf{E} the magnetic and electric fields respectively. This equation is solved with the use of a relativistic version of the Boris-method [22]. Potentially, this method allows us to introduce multiple particle species. However, for the simulations described in

this paper, we will only consider supra-thermal ions. The electrons are considered to be in thermal equilibrium and part of the thermal plasma that is treated through the MHD equations.

The same force, acting in the opposite direction, is applied to the equation of motion of the thermal fluid. Furthermore, the presence of supra-thermal particles influences the electric field, leading to a change in Ohm's law [11, 15], which becomes:

$$c \mathbf{E} = -((1 - R) \mathbf{v} + R \mathbf{u}) \times \mathbf{B}, \quad (2)$$

with \mathbf{v} the velocity of the thermal plasma, \mathbf{u} the supra-thermal particle velocity, which is obtained by averaging the velocities of the particles in the grid cell, and R the ratio of supra-thermal particles to the total particle density. It should be noted that this approach relies on the condition that the supra-thermal particle density remains low compared to the thermal plasma density. In situations where this condition does not apply, the PI[MHD]C method as described here becomes unreliable. For a full derivation of the relevant equations, we refer to [11, 15].

In [15] this method was used to successfully reproduce the results obtained by [11] using a similar approach, as well as the PIC-hybrid results obtained for comparable physical conditions by [12–14]). We now apply this method to a new parameter space, which, until now, has been left largely unexplored.

For our simulations, we use the same input conditions as [16]. However, because of the different method, we changed the initial setup. Instead of aiming a beam of plasma at a reflective wall and following the shock as it moves backward into the flow, we simulate in the frame of reference of the shock, following the general setup from [15]. We start the simulation from the analytic solution of the Rankine-Hugoniot conditions for an exclusively thermal plasma. From that point we start to inject supra-thermal ions with the injection rate found by [16] with an injection velocity of three times the pre-shock velocity of the thermal gas, conform [11, 15]. All particles are injected at the shock, which starts at $x = 0$. Over time, we adjust the point of injection to compensate for the motion of the shock and ensure that the ions are always injected at the shock location.

To demonstrate the effect of the Mach number on the particle acceleration process, we choose two simulations from [16]. One with $M_s = 2.0$ and $M_A = 18.2$ and one with $M_s = 3.2$ and $M_A = 29.2$. In both cases, we set the upstream magnetic field at a 13° angle with the direction of the flow. Because our method cannot duplicate the kinetic processes involved in the injection of particles into the DSA, we use an adhoc injection scheme in which particles with a fixed velocity, $v = 3v_{\text{shock}}$, and an isotropic velocity distribution in the post-shock rest frame, are injected immediately downstream of the shock location. For the $M_s = 3.2$, [16] found an injection rate of approximately $\xi = 4 \times 10^{-3}$, indicating that 4 out of every 1000 parti-

cles that cross the shock become supra-thermal. For the $M_s = 2.0$ the injection rate was 3×10^{-4} . We choose to keep the injection rate of the $M_s = 3.2$ shock found by [16]. However, in order to determine whether an increased injection rate might trigger particle acceleration in the case of the $M_s = 2.0$ shock, we choose instead to extrapolate along the injection rate found by for shocks above $M_s = 2.24$, which gives us an injection rate of 3×10^{-3} (See [16], Fig. 5.) All other input conditions are copied directly from [16], ensuring identical plasma- $\beta = 100$ for both simulations.

As our simulation box, we use a physical domain of $180 \times 30 R_l$, with R_l the Larmor radius of the particles at injection determined by the upstream magnetic field and the injection velocity. At its coarsest level, our grid has one grid cell per R_l and we allow for an additional three levels of refinement, which gives us an effective resolution of eight grid cells per R_l . The gas flows along the x-axis (long) from the upper boundary (right hand side in Figs. 1-2), where the inflow is set at a fixed rate, to the lower boundary, where it escapes from the simulation domain. It passes through the shock, which is initialized at $(x = 0)$. For the inflow velocity we copy the values from [16], which are set to $v = 0.027c$ for the $M_s = 2.0$ shock and $v = 0.052c$ for the $M_s = 3.2$ shock. The boundaries along the perpendicular direction (y-axis) are set to be periodic for both the thermal gas and the supra-thermal particles.

The total simulation time is equal to $20\,000 R_l/c$ and we start injecting particles at $t = 1000 R_l/c$ in order to give the shock a brief period to relax from the initial analytic solution to the solution found by the computational approach. Over this period we inject a total of 10 million supra-thermal particles with the individual particle mass and charge weighted to reflect the injection rate. Note that all injected particles are protons as we assume the electron plasma to be fully thermalized at all times. As the simulation progresses, we follow the location of the shock in order to ensure that the particles are always injected within on Larmor radius downstream of the shock.

3. Results

Figure 1 shows the magnetic field strength relative to the unperturbed upstream magnetic field (B_0), the thermal gas density relative to the unperturbed upstream thermal gas density (ρ_0) and the ratio between supra-thermal and thermal gas q/ρ (in our normalized units the proton charge q and mass m_p are equal), as well as the magnetic field lines for the $M_s = 2.0$ shock model after 2000 (left panel) and $19\,000 R_l/c$ (right panel) since the initial injection of supra-thermal particles. After $1000 R_l/c$, the introduction of supra-thermal particles has caused a small perturbation in the magnetic field strength, both upstream and downstream of the shock, with the upstream perturbations showing a pattern reminiscent of the perturbations in the mag-

netic field strength found by [12] for strong, semi-parallel shocks. However, the magnetic field amplification is small (typically of the order of ten percent) and the magnetic field lines remain unperturbed. After $19\,000 R_l/c$ the situation remains unchanged with the magnetic field amplification having been reduced somewhat compared to the earlier snapshot. Under these circumstances DSA can not take place because the upstream magnetic field lacks the ability to reflect particles back toward the shock.

In contrast, the $M_s = 3.2$ shows fluctuations in the direction of the upstream magnetic field, as well as its strength (See Fig. 2). Although initially (left panel) the fluctuations in the magnetic field strength appear similar to those for the $M_s = 2.0$ shock, the upstream magnetic field lines are showing small perturbations as well. In the later snapshot (right panel), the upstream magnetic field is clearly perturbed in both strength and direction and the downstream magnetic field has become turbulent. In this environment, we can expect particles to be reflected by the magnetic field, which will allow the shock to accelerate them.

Unlike the high-Mach shocks shown in [15], neither the $M_s = 2.0$ nor the $M_s = 3.2$ shock show significant corrugation of the shock front. For the high-Mach shocks the corrugation was caused by variations in pressure of the upstream medium as it passed through the shock front. The weak shocks shown here do not exhibit such strong perturbations because the high thermal pressure counteracts local compression of the gas. As a result, the ram pressure does not vary significantly along the plane of the shock. Similarly, the perturbations of the downstream medium are much weaker than what was found for the high-Mach shocks. This also influences the magnetic field amplification, which requires compression of the thermal gas. Even for the $M_s = 3.2$ shock, the amplification does not go beyond a factor of approximately 4.5, small when compared to the factor 15+ obtained for a $M_s = 30$ shock with plasma- $\beta = 1$ [15]. Particularly in light of the fact that for the $M_s = 3.2$ shock the post-shock magnetic field is already amplified by a factor 1.2 compared to the pre-shock field owing to the compression of the perpendicular component by the shock.

In the case of the $M_s = 2.0$ simulation, the shape of the (small) instabilities remains the same over time, though the amplitude increases somewhat. Upstream, where the instability originates, it presents with a single, dominant wavelength. This effect was also shown and analysed in [15]. The perturbation of the upstream medium is dominated by a single wavelength, which is determined by the ratio between the upstream current of the non-thermal particles and the local magnetic field strength. As the perturbations pass through the shock into the downstream medium, their wavelength is reduced owing to the compression by the shock. For the $M_s = 2.0$ simulation this pattern remains the same over time.

Initially, the $M_s = 3.2$ simulation shows the same be-

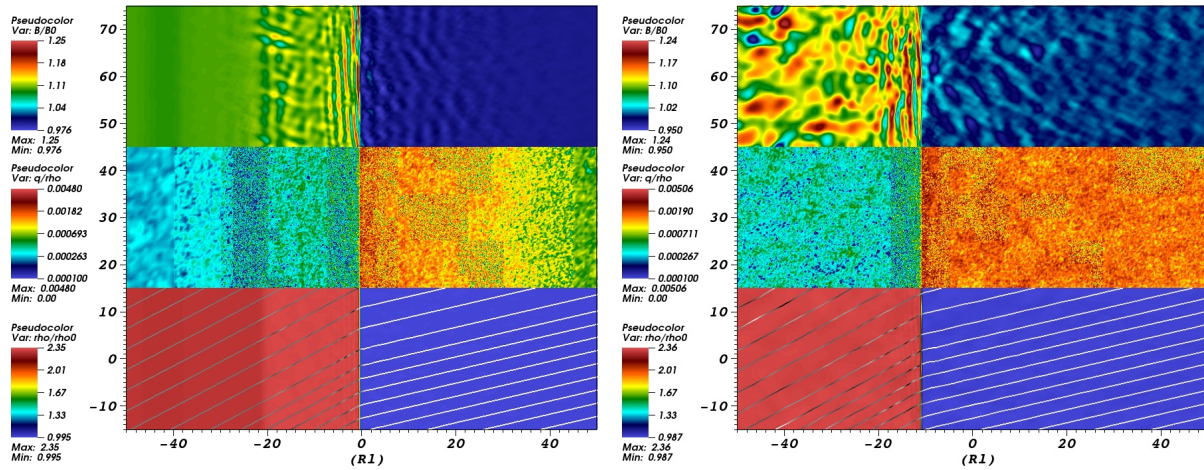


Fig. 1 Shock structure at the end of the simulation for a $M_s = 2.0$ shock after $1000 R_1/c$ (left) and $19000 R_1/c$ (left). From top to bottom, the magnetic field strength normalized to the unperturbed upstream magnetic field, the relative density of the supra-thermal particles relative to the thermal gas density, and the thermal gas density normalized to the unperturbed density of the inflow. The magnetic field lines are plotted on top of the thermal gas density. The gas moves through the simulation box from right to left. Although the simulations show a disturbance of the magnetic field strength, there is no change in the *direction* of the magnetic field lines.

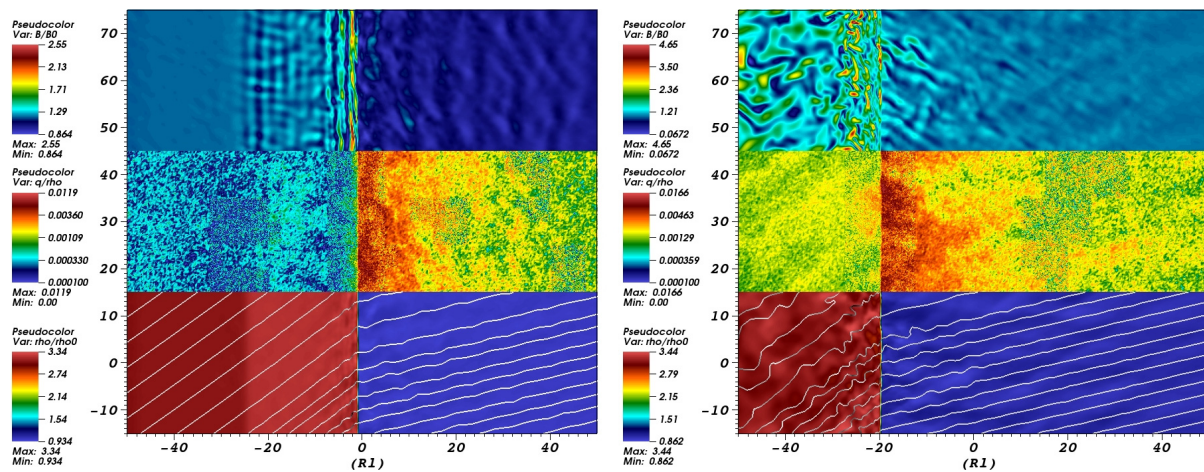


Fig. 2 Similar to Fig. 1, but for $M_s = 3.2$ simulation. initially (left panel) the disturbance of the magnetic field seems similar to what was observed for the $M_s = 2.0$ shock case. However, over time, the downstream magnetic field shows clear evidence of turbulence and the magnetic field lines are perturbed both upstream downstream of the shock.

haviour. However, this changes over time. Upstream, the instabilities are strong enough to cause a variation in the ratio between the (perturbed) local magnetic field and the upstream current. This in turn causes the preferred wavelength of the instability to vary, making the upstream wave-pattern less regular. Downstream, the instabilities become increasingly randomly turbulent partially because the fluctuations coming from the upstream medium are no longer dominated by a single wavelength, but also because these instabilities continue to interact with the non-thermal particles, causing further variation.

Note that these are MHD instabilities. The micro-turbulence involved in the injection process, as found in PIC simulations (See e.g. [16]), does not appear in our sim-

ulations, because this would require treating the electrons as particles, which we do not do. As we discussed briefly in Sec. 1, the acceleration of supra-thermal particles by a shock is a multistep process. Micro-turbulence makes it possible for the particles to accelerate through the SDA process until they reach a velocity equal to several times the pre-shock velocity of the upstream medium. In our simulations, we take this first step for granted and assume that the micro-turbulence is being effective in accelerating particles, as justified by the results of [16]. This assumption allows us to inject the particles at a speed of three times the pre-shock velocity, conforming to the velocity they would have had, if they had gone through the SDA process. Further acceleration requires the DSA process in

which particles interact with instabilities with longer wavelengths, which is where the MHD instabilities shown in this work become important.

4. Particle Spectra

Figure 3 shows the particle spectra obtained through our simulations. This plot shows the energy distribution of all particles in the simulation box at the end of the simulation. In the case of the $M_s = 2.0$ shock, the particle energy is distributed nearly symmetrically around the injection energy (E_0), showing that no significant particle acceleration is taking place. On the other hand, the $M_s = 3.2$ shock has produced particles with energies up to an order of magnitude higher than the injection energy, a clear indication that DSA has occurred.

Although the $M_s = 3.2$ shows clear evidence of particle acceleration, it is somewhat less efficient than the comparable PIC simulation by [16]. In the case of DSA, the particle spectrum is expected to follow a power law [5]. However, in our case, this is only the case for the range of $E = 1.5 E_0$ to $E = 2.5 E_0$, after which the number of particles per energy bin drops rapidly. This can be contributed to a combination of several factors: 1) We assume that the particle velocity at injection is isotropic in the rest frame of the post-shock gas, in reality, the transition from thermal to supra-thermal speed is the result of a complicated process that would not result in an isotropic distribution. As a result, many of our particles, launched initially in the downstream direction will never pass through the shock and therefore don't contribute to the acceleration process, reducing the *effective* acceleration rate. This was not a major issue in the case of the strong shock models [15], where the post-shock turbulence was strong enough to re-

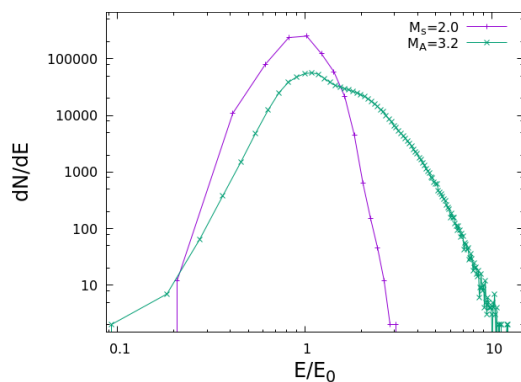


Fig. 3 Particle spectra for the $M_s = 2.0$ (purple) and $M_s = 3.2$ (green) shocks, showing the binned number of particles as a function of the energy relative to the injection energy (E_0). The $M_s = 2.0$ shock shows no significant particle acceleration, the particle energy being distributed nearly symmetrically around the injection energy. For the $M_s = 3.2$ shock, the particles are being accelerated, reaching energies of up to ten times the injection energy.

flect these particles back toward the shock, but in the case of the weak-shock model, the turbulent zone is thinner and the local magnetic field amplification relatively small. 2) Although we initialize the shock at $M_s = 3.2$, this value does not remain constant for the duration of the simulation. When we inject particles in the post-shock medium, we subtract their mass, momentum, and energy from the local thermal plasma to ensure that these quantities are conserved. This leads to a small reduction of the post-shock pressure. The post-shock gas then loses additional energy to the acceleration process, further reducing the pressure. As a result, the shock is weaker, and the compression rate across the shock is smaller than the values derived from the initial Rankine-Hugoniot solution. 3) Most importantly, because of the limited size of our simulation box, particles can escape downstream. This is impossible with PIC simulations, which use a reflective boundary downstream of the shock. Because the fastest particles are the most likely to reach the boundary, rather than being reflected by the magnetic field, they are more likely to escape, preferentially removing them from the spectrum.

5. Conclusions

Even with the artificially inflated injection rate, the $M_s = 2.0$ shock fails to accelerate the supra-thermal particles to a significant degree, whereas the $M_s = 3.2$ simulation shows clear evidence of particle acceleration. This confirms the results found by [16] and shows that the PI[MHD]C method can be used successfully to investigate these type of shocks. Moreover, its lower computational cost allows us to run 2-D simulations with a significantly larger domain along the axis perpendicular to the flow.

However, the energy interval over which DSA can be seen in our simulations is insufficient to obtain a reliable number for the energy loss to CRs in these shocks, which can be compared to the upper limit indicated by the observations. In the future, we will extend our simulations to cover the parameter space from $M_s = 2.0$ -4.0, while maintaining the high plasma- β , following the models presented by [16]. We will also increase the box size of our simulations in the direction parallel to the flow. This will allow the particles to continue, rather than escape from the box as occurs in our current model.

We also intend to explore the influence of the time-dependence of the injection rate. The results obtained by [16] show that the injection rate is not constant but decreases with time. We intend to include this effect in the future and use the ability of the PI[MHD]C code to simulate the shock over long periods of time to investigate how the changes in the injection rate influence the behaviour of the shocks and the particle acceleration process.

Acknowledgments

This research was supported by the National Research Foundation (NRF) of Korea through grant

2016R1A5A1013277 and by the Basic Science Research Program through the National Research Foundation of Korea (NRF) funded by the Ministry of Education, Science and Technology (2018R1D1A1B07044060).

- [1] F. Miniati, D. Ryu, H. Kang, T.W. Jones, R. Cen and J.P. Ostriker, *Astrophys. J.* **542**, 608 (2000).
- [2] D. Ryu, H. Kang, E. Hallman and T.W. Jone, *Astrophys. J.* **593**, 599 (2003).
- [3] A.R. Bell, *Mon. Not. R. Astron. Soc.* **182**, 147 (1978).
- [4] R.D. Blandford and J.P. Ostriker, *Astrophys. J. Lett.* **221**, L29 (1978).
- [5] L.O'C. Drury, *Rep. Prog. Phys.* **46**, 973 (1983).
- [6] A. Pinzke and C. Pfrommer, *Mon. Not. R. Astron. Soc.* **409**, 449 (2010).
- [7] F. Zandanel and S. Ando, *Mon. Not. R. Astron. Soc.* **440**, 663 (2014).
- [8] H. Kang and D. Ryu, *Astrophys. J.* **856**, 33 (2018).
- [9] M. Ackermann, M. Ajello, A. Allafort *et al.*, *Astrophys. J. Lett.* **819**, 149 (2016).
- [10] F. Vazza, M. Brüggen, D. Wittor *et al.*, *Mon. Not. R. Astron. Soc.* **459**, 70 (2016).
- [11] X.-N. Bai, D. Caprioli, L. Sironi and A. Spitkovsky, *Astrophys. J.* **809**, 55 (2015).
- [12] D. Caprioli and A. Spitkovsky, *Astrophys. J.* **783**, 91 (2014a).
- [13] D. Caprioli and A. Spitkovsky, *Astrophys. J.* **94**, 46 (2014b).
- [14] D. Caprioli, A. Pop and A. Spitkovsky, *Astrophys. J. Lett.* **798**, 28 (2015).
- [15] A.J. van Marle, F. Casse and A. Marcowith, *Mon. Not. R. Astron. Soc.* **473**, 3394 (2018).
- [16] J.-H. Ha, D. Ryu, H. Kang and A.J. van Marle, *Astrophys. J.* **864**, 105 (2018).
- [17] J.P. Edmiston and C.F. Kennel, *Plasma Phys.* **32**, 429 (1984).
- [18] B. Reville, S. O'Sullivan, P. Duffy and J.G. Kirk, *Mon. Not. R. Astron. Soc.* **386**, 509 (2013).
- [19] B. Reville and A. Bell, *Mon. Not. R. Astron. Soc.* **430**, 2873 (2013).
- [20] B. van der Holst, B.R. Keppens and Z. Meliani, *Comput. Phys. Commun.* **179**, 617 (2008).
- [21] M.S. Shephard and M.K. Georges, *Int. J. Numer. Methods Eng.* **32**, 709 (1991).
- [22] C.K. Birdsall and A.B. Langdon, *Plasma Physics via Computer Simulation* (The Adam Hilger Series on Plasma Physics, edited by C. Birdsall and A. Langdon. Adam Hilger, Bristol, England, 1991).